



This is a repository copy of *The effect of powder age in high speed sintering of poly(propylene)*.

White Rose Research Online URL for this paper:
<https://eprints.whiterose.ac.uk/174913/>

Version: Accepted Version

Article:

Williams, R.J., Fox, L. and Majewski, C. orcid.org/0000-0003-3324-3511 (2021) The effect of powder age in high speed sintering of poly(propylene). *Rapid Prototyping Journal*, 27 (4). pp. 707-719. ISSN 1355-2546

<https://doi.org/10.1108/RPJ-05-2020-0090>

This author accepted manuscript is deposited under a Creative Commons Attribution Non-commercial 4.0 International (<http://creativecommons.org/licenses/by-nc/4.0/>) licence. This means that anyone may distribute, adapt, and build upon the work for non-commercial purposes, subject to full attribution. If you wish to use this manuscript for commercial purposes, please contact permissions@emerald.com

Reuse

This article is distributed under the terms of the Creative Commons Attribution-NonCommercial (CC BY-NC) licence. This licence allows you to remix, tweak, and build upon this work non-commercially, and any new works must also acknowledge the authors and be non-commercial. You don't have to license any derivative works on the same terms. More information and the full terms of the licence here:
<https://creativecommons.org/licenses/>

Takedown

If you consider content in White Rose Research Online to be in breach of UK law, please notify us by emailing eprints@whiterose.ac.uk including the URL of the record and the reason for the withdrawal request.



eprints@whiterose.ac.uk
<https://eprints.whiterose.ac.uk/>

1 Structured Abstract

Purpose

This work aims to demonstrate for the first time that the cheap, commodity polymer, poly(propylene), can be successfully processed using High Speed Sintering, and that it can be recycled several times through the process with little to no detriment to either the polymer itself, or the parts obtained. This is significant as a step towards the realisation of High Speed Sintering as a technology for high-volume manufacturing.

Design/methodology/approach

A poly(propylene) powder designed for laser sintering was used to build parts on a High Speed Sintering machine. The unsintered powder was then collected and reused. Repeating this process allowed creation of seven generations of aged powder. A variety of characterisation techniques were then used to measure polymer, powder, and part properties for each generation in order to discern any effects arising from ageing in the machine.

Findings

It was found that poly(propylene) could be used successfully in High Speed Sintering, albeit with a low build success rate. Increased powder age was found to correlate to an increase in the build success rate, changes in microscopic and bulk powder properties, and improvement to the dimensional accuracy of the parts obtained. In contrast, no discernible correlations were seen between powder age and polymer molecular weight, or between powder age and the tensile properties of parts.

Originality/value

This is the first report of the use of poly(propylene) in High Speed Sintering. It is also first study regarding powder recyclability in High Speed Sintering, both in general, and using poly(propylene) specifically.

2 Introduction

High Speed Sintering (HSS) is a novel powder bed fusion process used for the additive manufacturing (AM) of polymer parts. In HSS, an infrared-radiation-absorbing ink is printed onto a polymer powder bed to create 2D cross-sections which are sintered selectively when an infrared (IR) lamp is passed over the bed. After each printing/sintering cycle, a new layer of powder is deposited onto the bed, and the process is repeated. After multiple repetitions, complex, 3D polymer parts can be obtained. During a build, the powder bed is maintained at relatively high temperatures in order to reduce shrinkage of the sintered areas, which would cause part warpage. This process is illustrated in Figure 1.

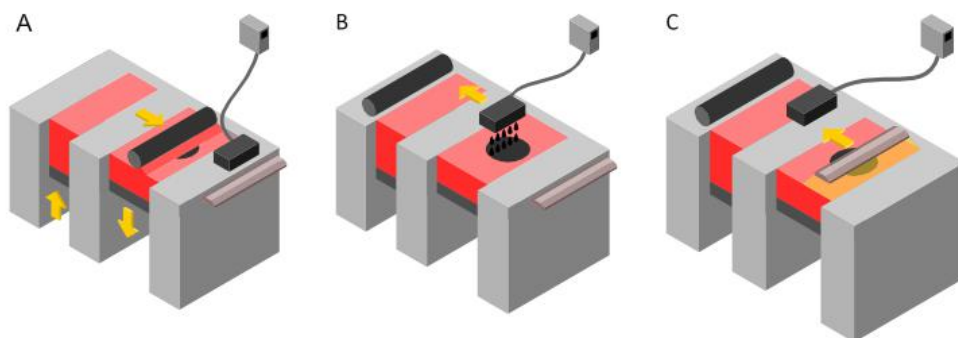


Figure 1: An illustration of the HSS process. First, a layer of powder is deposited on the build bed (A), then IR-absorbing ink is printed in the desired cross-section (B), and finally an IR lamp is passed over the powder bed (C), selectively sintering the ink-coated area. It should be noted that the powder delivery mechanism illustrated is slightly different to that in the machine used in this work, which deposits powder onto the build bed directly from an overhead hopper, rather than delivering it from a separate feed bed. This image was produced by Theo Doncaster.

The majority of polymers used in powder bed fusion processes like HSS are semi-crystalline, and the bed temperature is kept at a temperature between the crystallisation and melting points of the polymer being sintered; were the polymer allowed to cool and begin to crystallise, significant shrinkage would occur. HSS is a similar technology to the more-recently-developed multi-jet fusion (MJF) (O'Connor *et al.*, 2018), which relies on the same principles, but uses a different printing system to enable easier and more advanced post-processing of parts once built. Many of the aspects of HSS are also similar to the better-established technique of laser sintering (LS). Both HSS and LS, which are powder bed fusion techniques, rely on layer-by-layer assembly of parts in heated polymer powder beds, but in LS each layer is sintered by scanning an IR laser across the bed surface in the desired cross-section (Ligon *et al.*, 2017). The laser energy input is intense, and certainly much more intense than the relatively mild application of the IR lamp in HSS. As such, LS must be carried out under inert atmosphere to prevent powder oxidation (Ligon *et al.*, 2017), whereas HSS can be carried out under ambient atmosphere. While LS is much more widely-used and better understood than HSS, there are nonetheless some important manufacturing applications for which HSS has the potential to be better suited than LS.

Since its inception, one of the principal goals of HSS development has been to achieve economically-viable, high-volume production of polymer parts. In 2003, Hopkinson and Dickens calculated that the AM techniques available at the time could theoretically be cheaper than injection molding (IM) specifically, but only for relatively small production volumes (of the order of thousands) (Hopkinson and Dickens, 2003). Of the AM techniques studied, they concluded that the one most suitable for high-volume production was LS, which could be cheaper than IM for production volumes up to around 14,000 units for certain parts (Hopkinson and Dickens, 2003). They identified the high cost of LS machines and the relatively slow rate of production as major factors contributing to the price of parts made by the process, and HSS was subsequently developed to address these issues (Hopkinson and Erasenthiran, 2004; Thomas *et al.*, 2006). HSS has the potential for faster rates of part production than LS; in LS, the time required to sinter each layer is a function of the area of the cross-section being sintered, and production rate is hence

dependent on laser scan speed, but in HSS this layer time is independent of the area of each cross-section, since the printing and sintering lamp stroke speeds are the same regardless of the area of ink being printed on the bed (Thomas *et al.*, 2006). Achieving economically-viable, high-volume production with an AM technique like HSS is desirable since it would allow the expansion of AM principles (e.g. design freedom and flexible manufacturing) to markets such as fast-moving consumer goods (FMCGs), which remain dominated by more traditional manufacturing techniques.

However, there are a number of yet-to-be-resolved issues which prevent the adoption of HSS as a method for high-volume production of FMCGs. Not least among these is the limited range of materials which can be successfully processed using HSS. Thus far, research into HSS in particular has focused on high-value polymers, most notably poly(amide)s like Nylon-11 (Ellis *et al.*, 2015a) and Nylon-12 (PA12) (Majewski *et al.*, 2008; Ellis *et al.*, 2014b; Craft *et al.*, 2018; Fox *et al.*, 2015; Ellis *et al.*, 2014a), as well as some nylon-derived elastomers (Ellis *et al.*, 2014a, 2015b). PA12 in particular occupies a significant proportion of the polymer sintering market in general, largely because its thermal properties align well with the requirements for such processes (Craft *et al.*, 2018; Ligon *et al.*, 2017). More specifically, PA12 is a semi-crystalline polymer with a wide gap between melting and crystallisation temperatures, and a relatively high enthalpy of melting. This wide temperature range helps to prevent recrystallisation and shrinkage during a build (Craft *et al.*, 2018; Chen *et al.*, 2018), which would cause part warpage, while the relatively high enthalpy of melting limits unwanted sintering of powder away from the desired cross-section (Chen *et al.*, 2018), which would reduce the dimensional accuracy of the parts obtained, and also increase the degree of post-processing required. In combination with these favourable processing characteristics, PA12 also has relatively robust mechanical properties and good chemical resistance (Funk *et al.*, 2016), which further enhances its usefulness.

Despite the advantages of using PA12 in polymer sintering, its high cost makes it undesirable for many applications. For example, PA12 is certainly too expensive to be adopted

for FMCGs, which typically use cheap commodity plastics. This problem is exacerbated by the fact that PA12 undergoes thermal ageing as unsintered powder is recycled through the sintering processes. That is to say, the inability to continually reuse unsintered powder from one build to the next leads to material wastage, and an associated increase in cost per part. In the case of PA12, it is well known that extended times at the bed temperatures used in LS causes polymer chain extension (Chen *et al.*, 2018; Wudy and Drummer, 2019), which leads to changes in polymer rheology and structure (Chen *et al.*, 2018; Pham *et al.*, 2008), and ultimately to deterioration in the surface finish (Pham *et al.*, 2008) and mechanical properties (Dadbakhsh *et al.*, 2017) of parts. Similar powder degradation would also be expected in HSS, since the powder bed is kept at temperatures similar to those used in LS (Ellis *et al.*, 2014a), and indeed it is speculated that the problem could be exacerbated by the fact that HSS is carried out under an oxidising atmosphere (i.e. air), rather than the inert, nitrogen atmospheres used in LS. For the application of polymer AM to high-volume manufacturing markets like FMCGs, the ideal material would also have robust mechanical and chemical properties, but additionally be both cheap and able to be continually recycled through the process without significant degradation.

In general, material selection for trial in HSS has typically been inspired by materials which are already known to be useful in LS, since both techniques require materials with similar powder rheology and thermal properties (Ellis *et al.*, 2014a). Among the polymers known to be processable by LS, poly(propylene) (PP) is particularly promising for high-volume production using HSS. PP is already widely used in FMCGs on account of its low cost, good chemical resistance, and reasonably robust mechanical properties. Furthermore, PP has already been shown to be useful in LS, with several studies reporting the manufacture of good quality PP parts by LS (Wegner, 2016; Drummer *et al.*, 2010; Zhu *et al.*, 2015; Kleijnen *et al.*, 2016; Ituarte *et al.*, 2018), although the exact part properties are dependent on the specific grade of PP powder used. For example, early research by Drummer *et al.* demonstrated that while they could produce PP parts by LS, the mechanical properties obtained were significantly lower than both comparable PA12 parts, and benchmark values for injection molded PP (Drummer *et al.*, 2010). The PP parts

made by LS had an average modulus of elasticity of around 2000 MPa, compared to over 2500 MPa for the injection molded parts, and a tensile-stress-at-break of around 30 MPa, versus over 50 MPa for IM (Drummer *et al.*, 2010). Significantly, PP parts made by LS were also much less ductile than those made using PA12: the PP and PA12 parts had a mean elongation-at-break (EaB) of around 4% and 14%, respectively (Drummer *et al.*, 2010). In contrast, Wegner found that a specially-developed PP powder (Rolaserit PP) could be printed with comparable ductility to PA12 (Wegner, 2016). Zhu *et al.* found that PP parts made by LS using a highly-spherical, low isotacticity powder (Trial Corporation) had lower ductility (120% versus 610%), but higher tensile modulus (600 MPa versus 350 MPa) and tensile strength (19.9 MPa versus 16.65 MPa) in comparison to parts made by IM, which they attributed to differences in the extent and type of crystallinity obtained via the different processes (Zhu *et al.*, 2015). To date there are no published reports of PP being used in HSS, but it is clear from the literature for LS that it is a promising material for this process.

In addition to the good quality parts that can be obtained by LS of PP (Wegner, 2016; Drummer *et al.*, 2010; Zhu *et al.*, 2015; Kleijnen *et al.*, 2016; Ituarte *et al.*, 2018), there is also some indication that PP should be more readily recyclable than PA12 (Wegner and Ünlü, 2016). More specifically, Wegner and Ünlü demonstrated that there were little differences in the densities, Young's moduli, and tensile strengths of parts made using either virgin, once-used, or refreshed (i.e. a 50/50 mixture of virgin/used) PP powders (Rolaserit PP) (Wegner and Ünlü, 2016). However, they did also observe a decrease in the EaB of the sintered parts with increasing powder age (Wegner and Ünlü, 2016). Similarly, the used powder was found to have a slightly lower packing density, and a slightly higher melt viscosity (although the sizes of the uncertainties in the rheology data make this difficult to state for certain) (Wegner and Ünlü, 2016). While Wegner and Ünlü did not perform detailed chemical or morphological analysis to confirm fundamental changes (or lack thereof) to the nature of the polymer or powder, from a chemical perspective, it makes sense that PP would be less susceptible to thermal ageing than PA12. This is because PA12 contains reactive end groups which can undergo condensation and subse-

quent polymer chain extension (Dadbakhsh *et al.*, 2017), but PP is not expected to contain reactive functional groups, and hence should be stable provided that it is kept significantly below its onset of thermal degradation (i.e. the temperature at which it starts to spontaneously oxidise in air). Since PP has been shown to recycle well through the LS sintering process (Wegner and Ünlü, 2016), there is no reason not expect the same to be true for HSS. However, as of yet, this has not been studied. In addition, Wegner and Ünlü only looked at a maximum of once-used PP powder, but it is probable that the material would have to be able to be recycled through the build process significantly more times for it to be truly economically-viable in high-volume manufacturing.

In this work, we report both the first use of PP in a developmental HSS machine, and the affect of recycling the powder up to seven times through the build process. More specifically, it is shown that a commercially available PP powder can be used to build good quality parts via HSS, and that while some microscopic and bulk powder properties do change with increasing powder age, recycling the powder seems to cause no significant detriment to the chemical or tensile properties of the final parts obtained.

3 Materials and Methods

3.1 Materials

Parts were manufactured from CP22 PP powder which was provided by Diamond Plastics GmbH. The ink used was JetStream PCO7774 from SunChemical.

3.2 Methods

3.2.1 Part manufacture

Each build file consisted of five tensile dogbone specimens and four rectangular prisms to be built in a single stack, which is illustrated in Figure 2. Unless otherwise specified, the part characterisation data reported in Section 4 are averages across all parts made in different builds, but using the same age of powder.

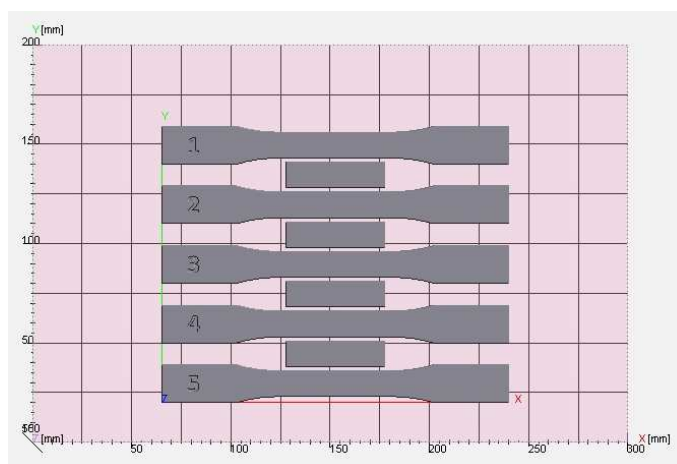


Figure 2: Top view (*x* and *y* direction) of the build layout as arranged in Rapix3D software.

These parts were manufactured using a voxeljet ‘alpha’ VX200 using the build parameters outlined in Table 1.

Table 1: The HSS build parameters used to manufacture parts from CP22.

Parameter	Setting used
Preheat power/%	50
Sinter power/%	100
Preheat speed/ mms^{-1}	60
Sinter speed/ mms^{-1}	105
Recoater vibration/%	100
Feed hopper fill frequency	11
Feed hopper fill duration/s	1.25
Grey level	3
Build bed temperature/ $^{\circ}\text{C}$	150
Build overhead/ $^{\circ}\text{C}$	150
Layer thickness/ μm	100

3.2.2 DSC

DSC data was obtained using a PerkinElmer DSC 8000. Approximately 7 mg of powder was measured for each sample. Temperature scans were carried out under nitrogen atmosphere using the following heating/cooling regime (with the heating scan being repeated twice): hold at 20 °C for 1 min; heat from 20 °C to 200 °C at 10 °Cmin⁻¹; hold at 200 °C for 1 min; cool from 200 °C to 20 °C at 10 °Cmin⁻¹.

3.2.3 GPC

GPC was carried out on behalf of the authors by Smithers Rapra. An Agilent PL GPC220 with 3 Agilent Technologies PLgel Olexis guard plus (300 mm, 13 µm) columns was used. Samples were dissolved in hot 1,2,4-trichlorobenzene with anti-oxidant added, and analysed at 160 °C with a flow rate of 1.0 mLmin⁻¹ using refractive index and differential pressure detectors. Calibration was carried out using polystyrene calibrants and Mark-Houwink parameters were used to equivocate to linear polypropylene.

3.2.4 Static light scattering

A Malvern Mastersizer 3000 and Hydro EV wet dispersion unit were used to measure the particle size of the powder via laser diffraction. The instrument used a HeNe laser (633 nm) and a visible LED (470 nm). The stirring and sonication were set to maximum (3500 rpm and 100%, respectively) for 900 s before measurement, then were adjusted to 200 rpm and 40% during data collection. The refractive index used for PP was 1.490 and the absorption index was set to 0.01. These variables were used in a Mie scattering model to calculate the particle size from the scattering data. Each run outputs the average of 10 measurements, and three runs were carried out for each sample. The Mastersizer was automatically aligned before each measurement and was cleaned between each measurement by rinsing three times with de-ionised water.

3.2.5 Microscopy

SEM images were captured using a Philips XL 30S FEG SEM with a beam operating voltage of 10 kV. Samples were prepared by adhering a monolayer of powder on carbon tape mounted on an SEM stub, which were then sputter-coated with gold.

Optical microscope images were captured in transmission mode using an Olympus BX50 microscope fitted with VisiCam 10.0 camera. The image scale was found by reference to an image of a graticule taken at the same magnification using the same instrument. Samples were prepared by placing a thin layer of powder on a glass slide.

3.2.6 Particle shape analysis

Particle shape factors were quantified using a Malvern Morphologi G3 fitted with an SPD1300 dry dispersion unit. In excess of 8500 powder particles were imaged for each sample, and the shape factors were output automatically by the Morphologi software.

3.2.7 Bulk tapped density

A 100 mL measuring cup was fitted with an extension piece that doubled its volume, and the cup was filled with excess powder. It was then placed on a mechanical contraption that allows the operator to tap the cup by 10 mm per tap. Using this apparatus, the sample was tapped 500 times. The extension sleeve was then removed and the excess compacted material was scraped off, leaving 100 mL of powder remaining in the measuring cup. This remaining powder was then weighed and the tapped density was calculated. This test was repeated three times for each powder age.

3.2.8 Elution time

A contraption consisting of a funnel with a relatively large orifice and removable stop below the orifice was made from PA12 by LS. The funnel was filled with excess powder,

and the excess was carefully scraped off the top to ensure that a repeatable volume of powder was used. The stop was then removed, and the elution time was measured as the time between removing the stop and complete elution of all the powder through the funnel. Five repeats of this measurement were carried out for each powder age. To limit variability, the experiment was conducted for all samples by the same operator and on the same day (at an ambient temperature of 19 °C, and relative humidity of 41%).

3.2.9 Shrinkage, wall growth and apparent density

Shrinkage and wall growth were quantified by measuring the dimensions of the tensile dogbones. More specifically, the lengths, gauge widths and tab widths of the dogbones were measured using digital calipers, and these values were plotted versus the corresponding values described in the CAD file. It should be noted that heights were not used (i.e. the z direction), since wall growth is not expected to occur to an equal extent on the top and bottom surfaces of the parts. Shrinkage and wall growth could then be calculated as described in Section 4.

The apparent densities of parts were found by measuring the dimensions of the rectangular prisms made during the builds, and using these dimensions to find part volume. Weighing each prism then allowed calculation of its apparent density.

3.2.10 Tensile testing

Tensile properties were measured according to ASTM D638-14. Type 1 tensile test pieces were used, as described in the standard. A Tinius Olsen H5K-S fitted with 500LC laser extensometer and Horizon software was used to measure tensile properties. Reflective tape was attached on the gauge length at an initial distance of 50 mm apart to allow the extensometer to detect the part and record its extension. The test speed was 5 (mm)min⁻¹, and the specimens generally failed after 0.5-5 min of testing time.

3.2.11 Statistical analysis

For each of the analysed dependent variables (UTS, Shrinkage, etc.), OriginLab software was used to conduct one-way ANOVA to identify whether any of the means of each powder age level (Virgin, Used 1, etc.) were significantly different at the 95% confidence interval. Simultaneously, post-hoc Scheffe tests were conducted to establish which, if any, of the levels were significantly different from one another.

4 Results and discussion

4.1 Correlations between polymer thermal properties and build success rates

HSS builds of PP parts were attempted using a commercially available PP powder, CP22 (Diamond Plastics GmbH), which has previously been shown to be processable by LS (Kleijnen *et al.*, 2016). The DSC trace for this powder is shown in Figure 3. The peak melt and crystallisation temperatures were found to be around 165 °C and 117 °C, respectively. This is similar to the results found in literature (Kleijnen *et al.*, 2016), and is lower than that of PA12. Since PA12 is already well-known to be readily able to be processed by HSS, the relatively lower melting point of this PP suggests that the energy input required to melt it should be achievable using HSS. Similarly, the window between melting and crystallisation peaks for the PP (around 48 °C) is comparable to that observed for PA12 (Chen *et al.*, 2018; Craft *et al.*, 2018), suggesting that CP22 PP should also readily be able to be sintered using HSS.

However, it can also be seen in Figure 3 that the onset of melting for the PP is broad, which has implications for the processing window of the powder. Because the IR lamp imparts energy to the whole powder bed during a sintering stroke, there is the possibility of powder being sintered away from the printed cross-section if the bed is being kept too

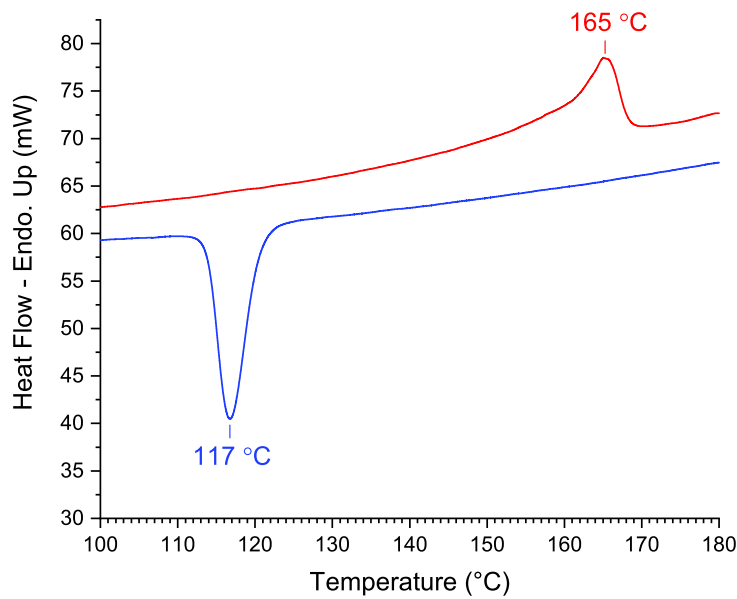


Figure 3: DSC data for CP22 PP powder. The material has a peak melting temperature of 165 °C, and a peak recrystallisation temperature of 117 °C. The onset of melting is broad, appearing to extend into the range of 150 °C.

close to onset of melting. However, the bed temperature also needs to be close enough to the melt onset that the energy imparted to the printed cross-section is sufficient to cause effective sintering. A broadening of the melt onset therefore means that the bed needs to be kept at a temperature relatively far away from the peak melt temperature, meaning that more energy is needed to cause sintering. In practice, this reduces the size of the process window. Indeed, it was found in this case that the build bed temperature needed to be kept at 150 °C, which is relatively far away from the peak melt temperature, and changing bed temperature by only ± 2 °C caused the build to fail. At the higher temperature, failure was caused by sintering of the unprinted areas on the bed making it impossible to retrieve parts, and failure at lower temperatures was caused parts cooling to the crystallisation temperature and warping/curling during the build (in some cases causing them to come into contact with the moving lamp and printheads above the bed). Even at a temperature of 150 °C, only 36% of the attempted builds were completed without failing in some way (i.e. without at least one of the parts failing). This high failure rate is probably due to the narrow processing window coupled with engineering limitations with regards to how

precisely and consistently the bed temperature can be maintained in the developmental machine. Nonetheless, the builds that did not fail produced good quality parts, some examples of which are shown in Figure 4.

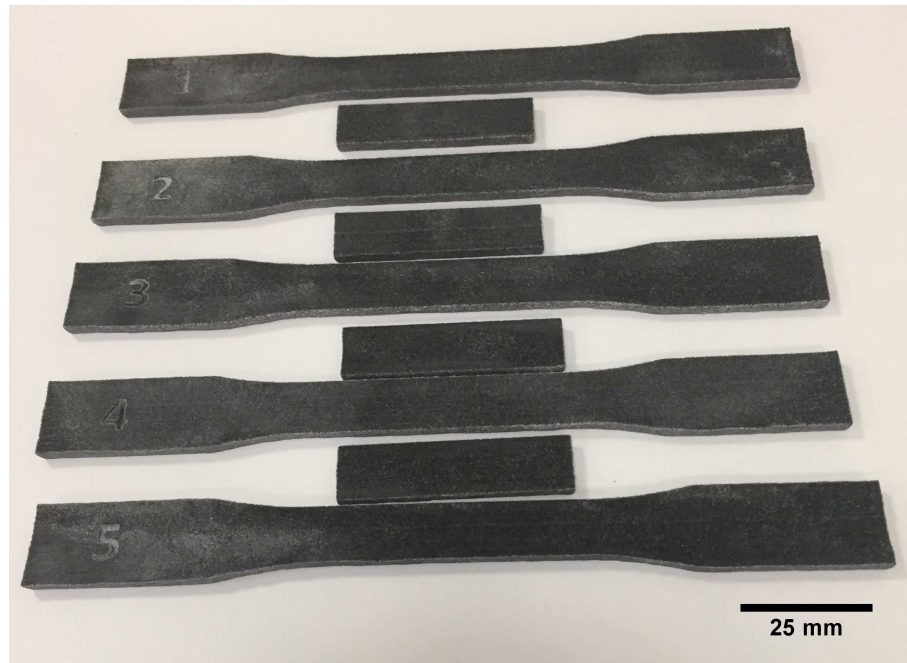


Figure 4: A selection of parts made by HSS of CP22 PP.

After each build, the unsintered powder surrounding the parts was collected and passed through a coarse sieve to remove or break up large aggregates. This recycled powder grade was then used in a subsequent HSS build. This workflow is illustrated graphically in Figure 5 for the sake of clarity. Repeating the cycle of building then recycling allowed the creation of seven generations of used powder. The process of recycling powder necessarily leads to the loss of some material; for example, larger aggregates are discarded during sieving, and some powder is always lost accidentally (e.g. through spillages). This means that the yield of usable powder decreases with increasing powder age. Nonetheless, the first six generations of powder generated were of sufficient quantity for parts to be built for tensile testing and for larger-scale powder characterisation (e.g. powder rheometry) in addition to small-scale characterisation (e.g. DSC) to be carried out. However, significantly fewer repeat builds could be carried out for older powder generations.

Interestingly, the build success rate seemed to increase with increasing powder age, as shown in Table 2. In the table, a build is listed as “complete” if no part failure was

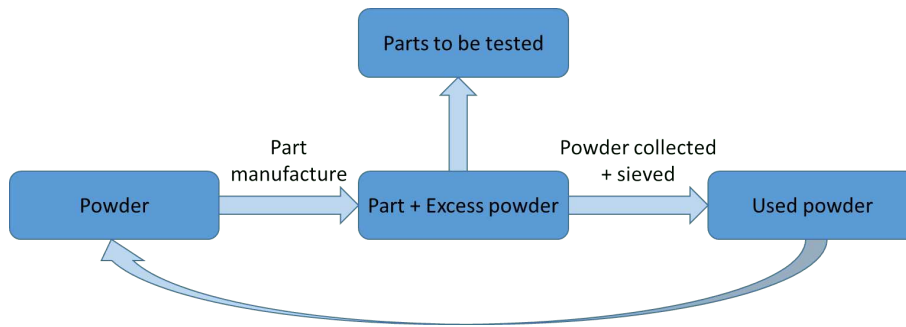


Figure 5: A graphical illustration of the process used to age powder in this work.

observed, “partially complete” if one part in the build failed, and “failed” if more than one part failed. Failure in these builds was caused by parts cooling and warping in the powder bed. For each complete build, five dogbone specimens were obtained for tensile testing and measuring dimensional accuracy, and four rectangular prism specimens were obtained for measuring density. For each partially complete build, one specimen failed, so either four dogbones and four prisms were obtained, or five dogbones and three prisms were obtained. The success rate shown in Table 2 is calculated by calculating the fraction of complete builds as a percentage of the total number of builds. While it is probable that the smaller number of builds for later generations of powders artificially inflates their build success rates, the data nonetheless suggest that used CP22 powder can actually be more readily processed in HSS than the virgin powder.

Table 2: The number of successful versus unsuccessful HSS builds for different generations of aged CP22 PP powder. Each successful build produced five dogbone specimens, and four rectangular prism specimens, and each partially successful build produced either four dogbones and four prisms, or five dogbones and three prisms.

Powder age	Total number of builds	Builds complete	Builds partially complete	Builds failed	Success rate
Virgin	11	4	2	5	36%
Used 1	7	1	5	1	14%
Used 2	7	1	5	1	14%
Used 3	6	5	0	1	83%
Used 4	4	4	0	0	100%
Used 5	2	2	0	0	100%
Used 6	1	1	0	0	100%

The increase in build success rate with increasing powder age roughly correlates to changes in the crystallinity of the polymer. To characterise the effect of powder age on crystallinity,

powder samples from each generation were analysed using DSC. This analysis included a second heating step after the initial heat and cool down, so as to allow comparison of the powders when they had the same thermal history. While the peak melting temperature was consistently lower for the second heat in all samples, it can be seen in Figure 6 that the melting temperatures for both heating runs and the crystallisation temperatures do not have an obvious dependence on powder age. However, as can be seen in Figure 7, the enthalpy (ΔH) of melting for the first heat increases with powder age from 80 Jg^{-1} up to around 112 Jg^{-1} after three uses (a difference of 32 Jg^{-1}), at which point it seemingly plateaus. There also appears to be a smaller change in the enthalpy of crystallisation, which decreases with increasing age (with a range of up to 12 Jg^{-1}), although this trend is less clear. There is no obvious change in the enthalpy of melting for the second heat, which would be expected since all of the samples have the same thermal history by that point. The enthalpy of melting is proportional to the extent of crystallinity, so it can be concluded that heating CP22 PP powder to the temperatures achieved in HSS increases the extent of crystallinity within the polymer, although it is unknown whether this occurs at the powder bed temperature maintained in the machine, or at the temperature achieved when the sintering lamp passes over the bed. It is also unknown whether the increase in crystallinity is an increase in the size or number of crystal domains. Therefore, while the first generation at which enthalpy of melting plateaus (Used 3) is also the first generation at which high build success rates begin to be seen, the physical connection between the two remains unclear.

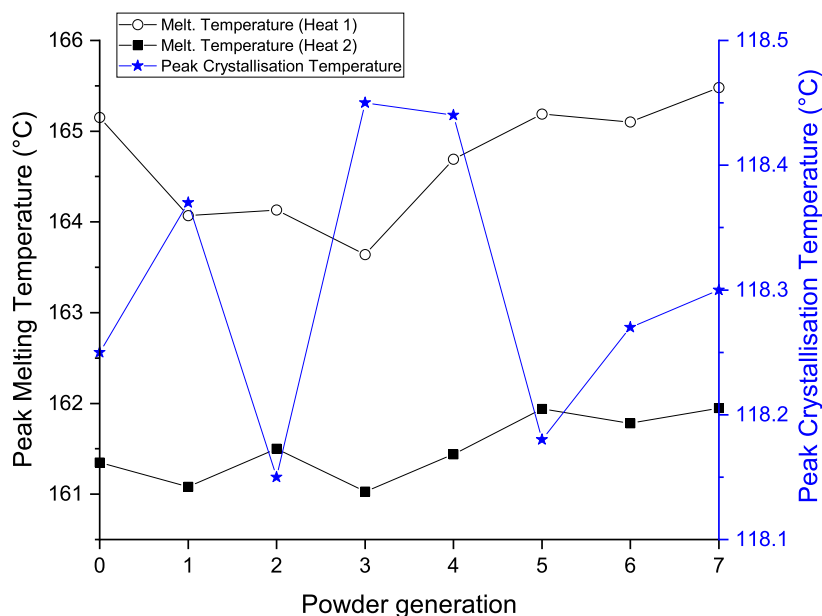


Figure 6: The peak melting temperatures (1st and 2nd heat) and crystallisation temperatures for CP22 at different stages of powder aging. Generation 0 is virgin powder. The lines between data points are included to help guide the reader's eye.

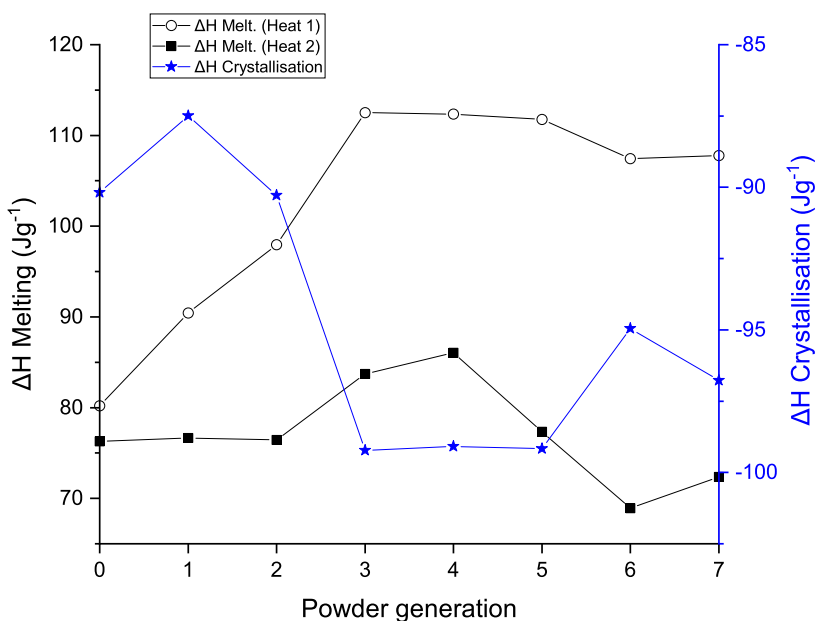


Figure 7: The enthalpies of melting (1st and 2nd heat) and crystallisation temperatures for CP22 at different stages of powder aging. Generation 0 is virgin powder. The lines between data points are included to help guide the reader's eye.

4.2 Effect of powder age on polymer molecular weight

Powder ageing clearly affects the crystallinity of the PP powder used, but it does not appear to affect its molecular structure. This is inferred from gel permeation chromatography (GPC) data, which indicates that there is no obvious dependency of polymer molecular weight or dispersity on the extent of powder ageing (Figure 8). More specifically, neither the number-average molecular weight (M_n), nor the weight-average molecular weight (M_w) seem to correlate to powder age. Similarly, the dispersity (\mathcal{D}) shows little change. While this technique is insensitive to functional group changes on the polymer (e.g. that might be caused by oxidation), it does demonstrate that no chain extension occurs in the PP as it is held at elevated bed temperatures. This is significant as chain extension is known to be a major cause of the deterioration of PA12 part properties as the powder is aged in LS (Chen *et al.*, 2018; Wudy and Drummer, 2019). Similarly, there is minimal evidence for a significant degree of chain scission (which would lead to a reduction in molecular weight). The relative inertness of PP in the powder bed seen here is an indication that it is indeed a more desirable material than PA12 for use in HSS where powder recyclability is important (e.g. high-volume manufacturing).

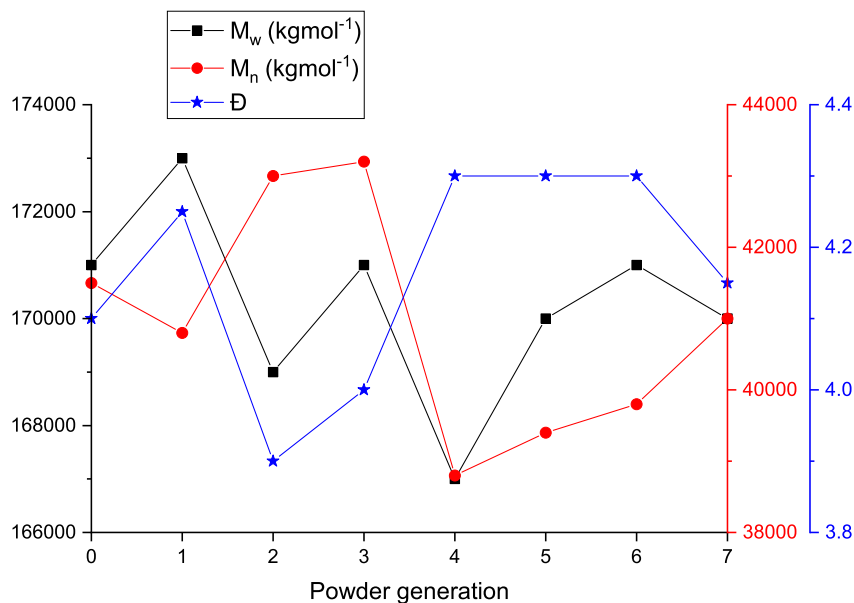


Figure 8: The molecular weight and dispersity of CP22 PP as a function of powder age. It can be seen that there is little change in the molecular weight of the polymer, suggesting that no chain extension is occurring. The lines between data points are included to help guide the reader's eye.

4.3 Effect of powder age on particle morphology

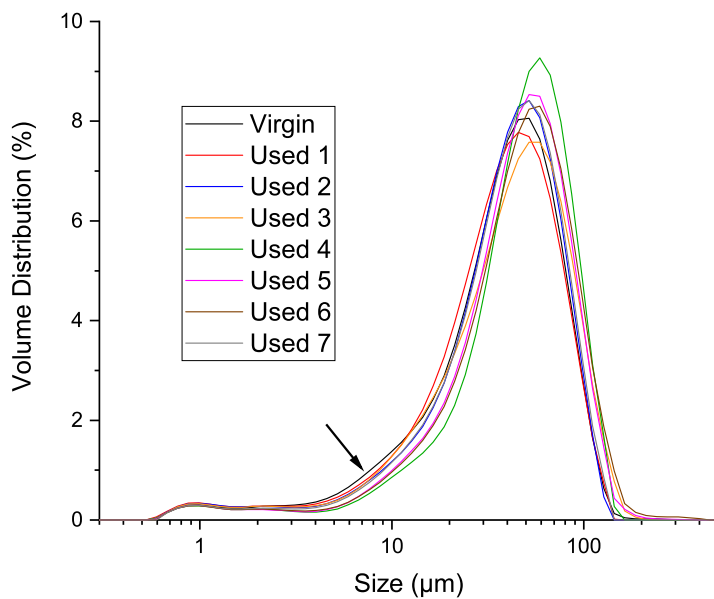
In contrast to polymer molecular weight, the particle size distribution of the powder was seen to change with increasing powder age. Laser diffraction was used to take measurements of particle size, and the volume distribution traces obtained from the scattering data are shown in Figure 9a. The distributions are similarly shaped, but there is a noticeable shoulder at small sizes on the main peak for the virgin powder, which suggests that there is a larger population of smaller particles in this sample. A more precise analysis can be achieved by studying the D10, D50, and D90 values for each distribution. These values represent the maximum particle size measured for the smallest 10%, 50%, and 90% of particles in each powder. Figure 9b shows the D10, D50, and D90 plotted against powder age, and it can be seen that the particle sizes increase continuously as the powder is recycled through the machine. By generation 7, the D10 had increased by about 4 μm , the D50 by about 10 μm , and the D90 by about 16 μm . Since the D values are measured with reference to certain percentiles in the number population of the particles, their increase can either represent an increase in the sizes of the particles, or the loss of smaller

particles (which would cause a larger particle size to occupy the 90th percentile etc.). Particles could increase in size if the powder were able to sinter to some extent away from the printed cross-sections. This could feasibly also cause loss of smaller particles if they were supported on the surfaces of larger particles, and fuse with the larger particle during sintering. However, loss of smaller particles without sintering could also occur if they are somehow aerosolised and lost during either the build or post-processing.

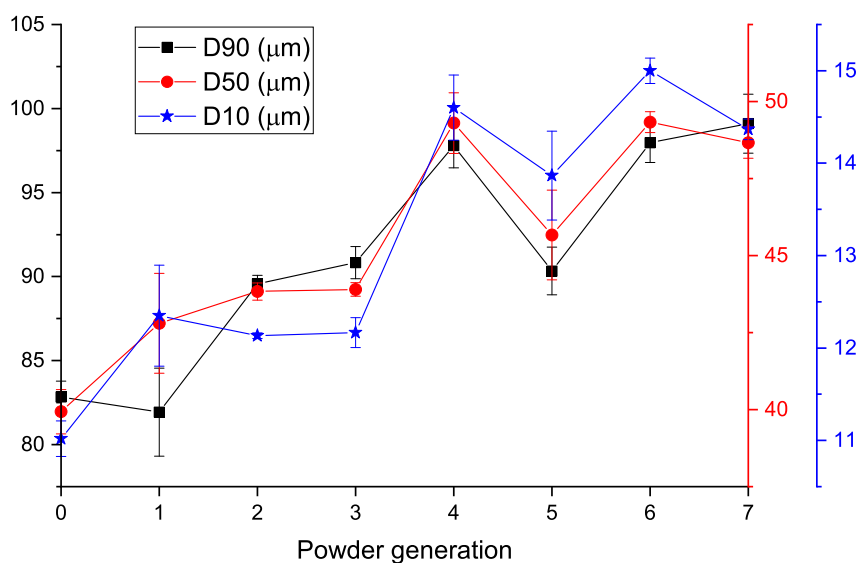
A possible way of identifying cause of the change in powder particle size would be to analyse the shapes of the particles. For example, were two particles incompletely sintered together, it might be expected that the resulting particle would be more elongated and less compact than either of the original constituents. Figure 10 shows SEM and optical microscope images of the virgin powder. It can be qualitatively stated that the particles are a range of shapes and sizes, with their rough surfaces readily apparent in SEM images. Also present are optically transparent, highly spherical objects. These are assumed to be additives which have been added to the polymer powder to enhance flow.

Quantification of particle shape was carried out using a Malvern Morphologi G3, which uses an optical microscope to image thousands of particles. These are then automatically analysed by the associated software to output values for the shape factors of the particles. The shape factors of interest here are: convexity (C), which is a measure of the surface roughness of the particles; high-sensitivity circularity (HSC), which is a measure of the compactness of the particles (i.e. how close they are to perfectly circular); and aspect ratio (AR), which is a measure of the elongation of the particles. The equations used to describe these properties are summarised in Table 3. For reference: a perfectly spherical, perfectly smooth object has a C of 1, a HSC of 1, and an AR of 1; a highly elongated, perfectly smooth object has a C of 1, but HSC and AR close to 0; and a highly elongated object with high surface roughness has values close to 0 for all three shape factors.

Distribution plots for the shape factors of the different generations of CP22 powder are shown in Figure 11. Only the virgin powder was discernibly different from the other generations of powder; it had larger populations at lower values for all three of C, HSC



(a)



(b)

Figure 9: The size distributions of virgin and aged CP22 powders obtained via laser diffraction (a), and the mean D10, D50, and D90 values obtained from these distributions plotted against powder age (b). It can be seen that the sizes of the powder samples increase, which can either be attributed to an increase in particle size, or a loss of small particles. The arrow in (a) indicates the peak shoulder at small particle sizes present in the virgin powder. The uncertainties in (b) are the standard errors of several measurements, and the lines between data points are included to help guide the reader's eye.

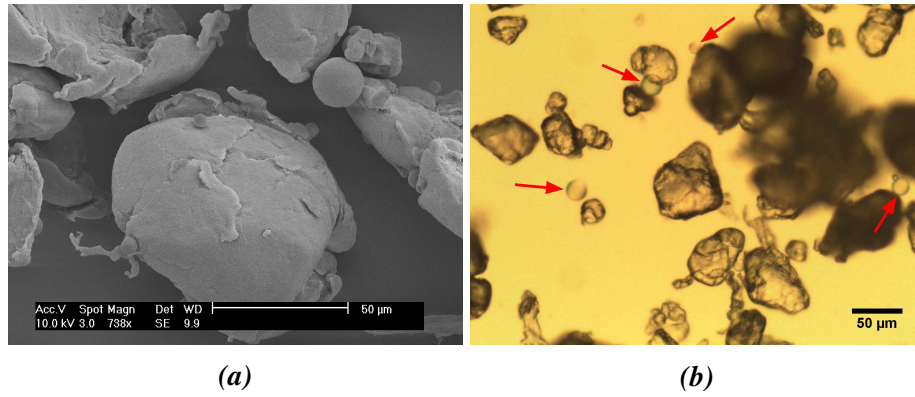


Figure 10: SEM (a) and optical microscope (b) images of virgin CP22 PP powder. The particles are irregular, and SEM in particular shows their rough surfaces. There are also some highly spherical objects (highlighted with red arrows in (b)), which are assumed to be additives used to enhance powder flow.

Table 3: Mathematical descriptions of the shape factors used to characterise the particles in CP22 PP powder.

Shape factor	Equation
Convexity	$C = \frac{\text{Convex hull perimeter}}{\text{Perimeter}}$
High-sensitivity circularity	$HSC = \frac{4\pi \times \text{Area}}{\text{Perimeter}^2}$
Aspect ratio	$AR = \frac{\text{Width}}{\text{Length}}$

and AR. This suggests that there are more rough, incompact, and elongated particles in the virgin powder, i.e. particle shapes in the virgin powder were more irregular. For the used powders, no obvious increase in the irregularity of the powder shapes was seen with increasing powder age, which is an increase that would be expected were large particles in the powder bed being sintered together during a HSS build. This is evidenced in Figure 12, which gives the mean values for all of the shape factors as functions of powder age. The apparent change in particle shape from relatively rough and incompact in the virgin powder, to relatively smooth and compact for the used powders can probably be attributed to some degree of annealing of the particles occurring in the hot powder bed, the extent of which has already maximised after use in one build. It cannot be concluded that larger particles sinter together in the powder bed, since this would be expected to lead to a continuous decrease in the shape factors with powder age. Similarly, the change in shape

is probably unrelated to the loss of additives during processing, as loss of these highly spherical objects would have also led to a decrease in the shape factors. However, it is still feasible that smaller particles supported on larger ones may extensively merge with their supports, which could increase particle size without leading to a significant change in shape.

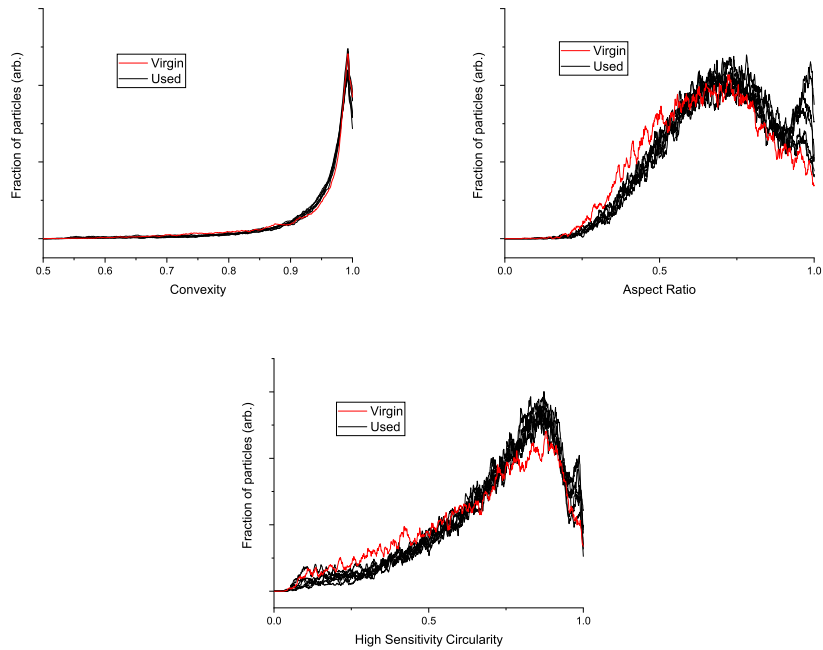


Figure 11: The distribution plots of the shape factors measured for virgin and aged CP22 powder. All generations are included on the graphs, but only the virgin powder (the red line) is distinguished from the rest as it was the only one which was discernibly different. It can be seen that the virgin powder has a larger population at lower values of all shape factors, suggesting that there are more rough and elongated particle shapes in this sample.

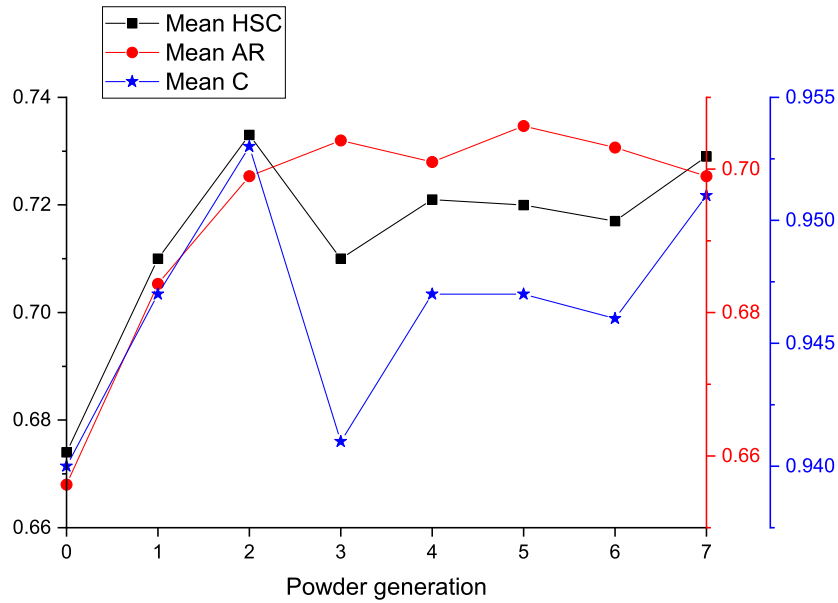
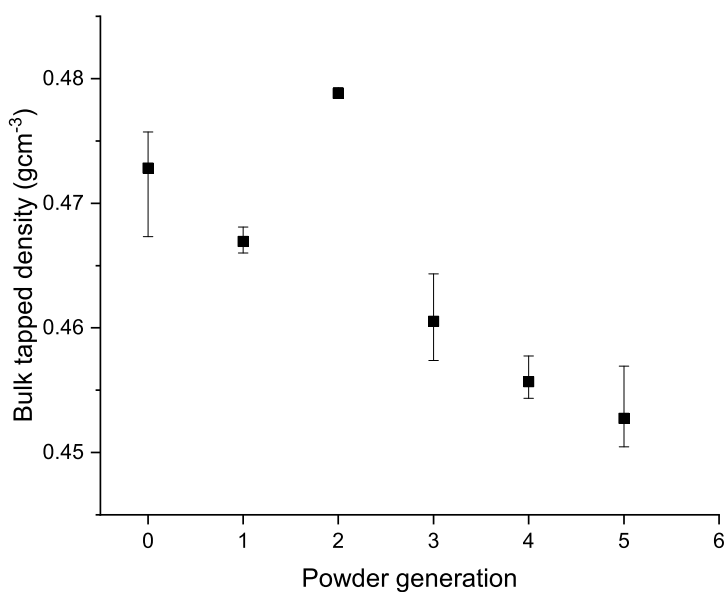


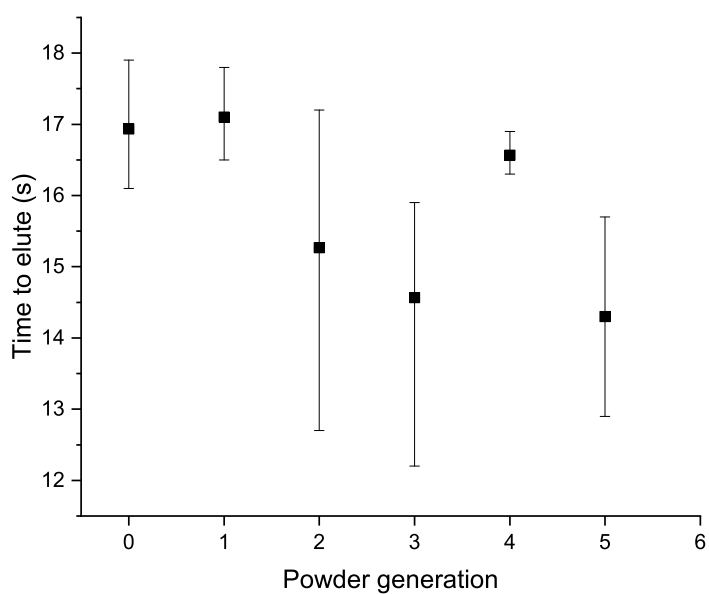
Figure 12: The mean values of shape factors for CP22 PP powder as functions of powder age. Apart from an apparent increase from virgin powder to Used 1, there is not an obvious dependency of any shape factor on powder age. The lines between data points are included to help guide the reader's eye.

4.4 Effect of powder age on bulk powder properties

Although there was no obvious change in the manner of powder deposition during the build, the change in microscopic powder particle properties did seem to affect the bulk properties of the powder. As can be seen in Figure 13a, the bulk tapped density of the powder decreased continuously with increasing powder age, from 0.47 gcm^{-3} for virgin powder to 0.45 gcm^{-3} for Used 5. Similarly, the time taken for powder to elute through a funnel appears to decrease as the powder ages (Figure 13b), from 17 s for virgin powder to around 14 s after five generations, although this trend is difficult to state for certain considering the large ranges of values measured for each sample. For both techniques, there was not sufficient powder of advanced age (Used 6 and Used 7) to allow for measurement. Nonetheless, it is reasonable to state that increasing CP22 PP powder age leads to both a continuous reduction in the density of the powder bed, and a continuous decrease in the effective viscosity of the powder. This is probably due to the increase in particle size with increasing age, which leads to poorer packing, and increased rates of powder flow (Fu *et al.*, 2012).



(a)



(b)

Figure 13: Mean values of bulk tapped density and powder elution time as functions of powder age. Both decrease with increased ageing, which is probably due to the increase in particle size. There was not sufficient powder available to measure past generation 5. The error bars in both sets of data represent the ranges of the measured values.

As would be expected, the decrease in the bulk density of powder led to a subsequent decrease in the densities of parts manufactured by HSS. This is illustrated in Figure 14, which shows the apparent density of the parts (i.e. the mass of each part divided by the volume calculated using its measured dimensions) plotted versus powder age. It can be seen that part density decreases in a similar manner to the bulk powder density (Figure 13a), going from 0.77 gcm^{-3} initially, to 0.71 gcm^{-3} when parts were built from Used 6 powder. The significance of these changes will depend on the application for which the parts are to be used; for example, the parts with lower densities are expected to be more porous, which may have implications for their permeability (and hence usefulness, e.g. in packaging applications).

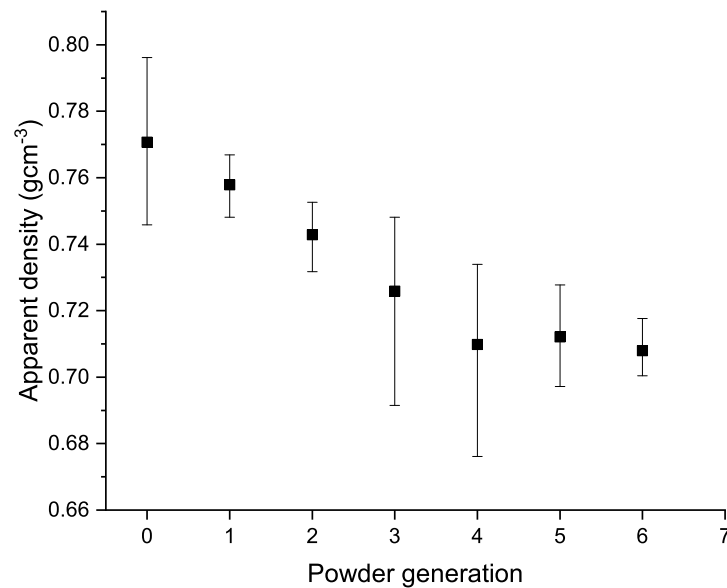


Figure 14: Mean apparent part density plotted against powder age. It can be seen that part density decreases with increasing powder age, which is a consequence of the decrease in bulk powder density. The error bars represent the ranges of the measured values.

4.5 Effect of powder age on the dimensional accuracy of parts

The change in powder properties also appears to lead to a increase in the dimensional accuracy of the parts built by HSS, i.e. a decrease in the difference between the actual

dimensions of the parts and the intended dimensions described in the CAD file. In HSS, changes in part dimensions are caused by two competing processes, namely shrinkage and wall growth. Shrinkage is the decrease in size caused by sintering and recrystallisation, and is a relative change (i.e. the change in a given dimension is dependent on its initial size). Wall growth is the increase in size caused by unwanted sintering to the part of powder adjacent to the printed cross-section. It is an absolute change since the extent of adjacent powder over which unwanted sintering can occur is independent of part dimensions. These processes are illustrated in Figure 15 for the sake of clarity.

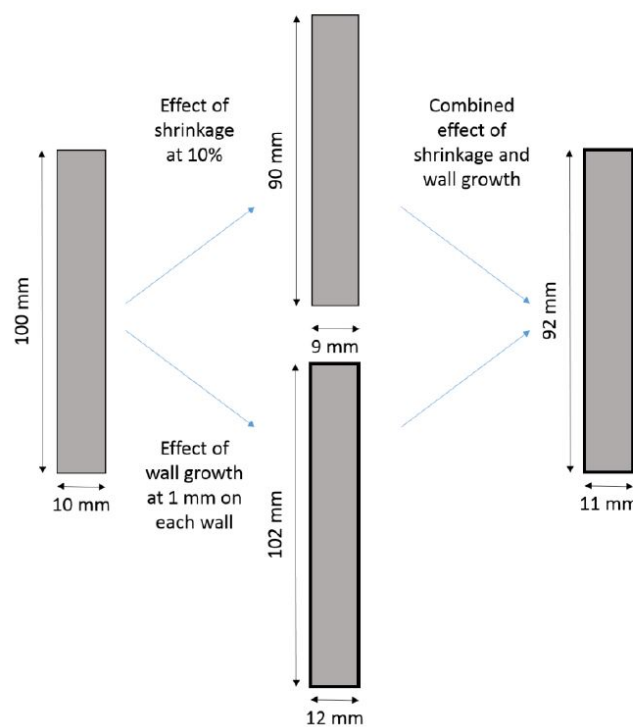


Figure 15: An illustration of the competing processes of shrinkage and wall growth that occur during HSS.

In practice, shrinkage and wall growth can be quantified by plotting the measured part dimensions against theoretical part dimensions (i.e. those defined in the CAD file). More specifically, such a plot can be fitted with a line of the form $y = mx + c$. Since shrinkage is proportional to dimension size, the gradient (m) of this line can be used to calculate it as per Equation 1. Because wall growth is independent of dimension size, its contribution to part dimensions is found using the y intercept (c) of the line as shown in Equation 2 (which addresses the fact that size measurements with calipers take into account two

walls). In this case, the dimensions that were measured to determine shrinkage and wall growth were the lengths, tab widths, and gauge widths of the dogbone specimens before they were subjected to tensile testing.

$$\text{Shrinkage (\%)} = 100(1 - m) \quad (1)$$

$$\text{Wall growth} = \frac{c}{2} \quad (2)$$

As can be seen in Figure 16, both shrinkage and wall growth decrease with increasing powder age: parts made using virgin powder had a shrinkage of 2.8% compared to 2.3% for Used 6, and wall growth decreases from 0.2 mm to effectively 0 mm from generation 4 onwards. This demonstrates that dimensional accuracy is better when aged powder is used. Indeed, by generation 4, wall growth has effectively been eliminated. The negative wall growth for generation 4 and later is probably an artefact of large variations between samples, as well as the uncertainty inherent in fitting a small number of data points (i.e. fitting a line to the three measured specimen dimensions). It is speculated that the decrease in wall growth could be caused by the larger particles packing less effectively against the part surfaces. Alternatively, the increase in enthalpy of melting seen with increasing powder age (Figure 7) could mean that the additional energy required to melt the particles at greater powder ages makes it less likely for sintering to occur away from the printed cross-section. Similarly, the increase in melt enthalpy could explain the decrease in shrinkage since it implies that later generations are more crystalline, and so when powder is deposited it is already close to the minimum size that can be achieved by recrystallisation alone. However, in the case of both shrinkage and wall growth, the large ranges make it difficult to state from inspection alone exactly which generations have different dimensional accuracy from one another (which would be useful, for example, to determine whether there is a critical powder age beyond which accuracy is maximised).

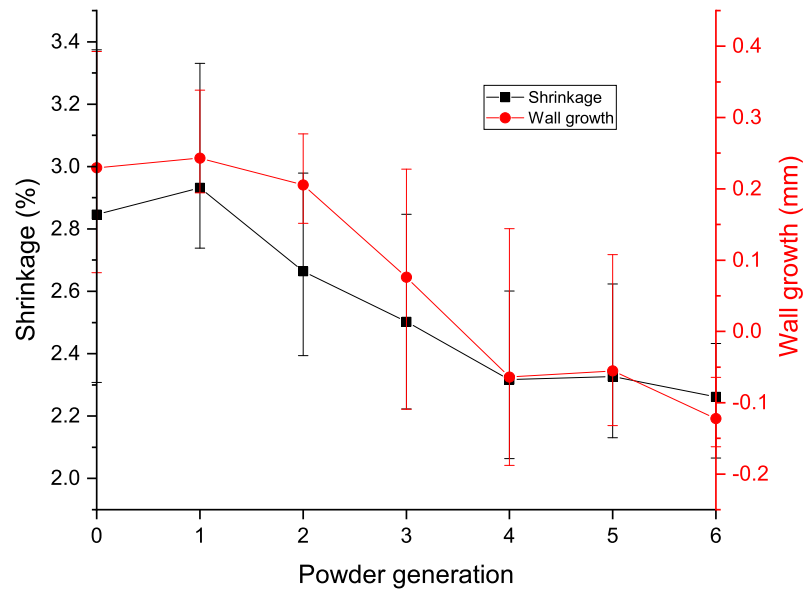


Figure 16: Mean shrinkage and wall growth as functions of powder age. Both quantities decrease with increasing age, and by generation 4 wall growth is almost nonexistent. The error bars are the ranges of measured values, and the lines between data points are included to help guide the reader's eye.

4.6 Effect of powder age on the mechanical properties of parts

While it can be concluded that powder age affects the dimensional accuracy of CP22 parts made by HSS, it did not obviously affect their mechanical properties. Tensile testing was performed on parts made using virgin and used powder, and their Young's moduli (YM), ultimate tensile strengths (UTS) and EaBs are shown in Figure 17. It can be seen that the large and frequently over-lapping uncertainties make it impossible to determine any trend for any of the mechanical properties.

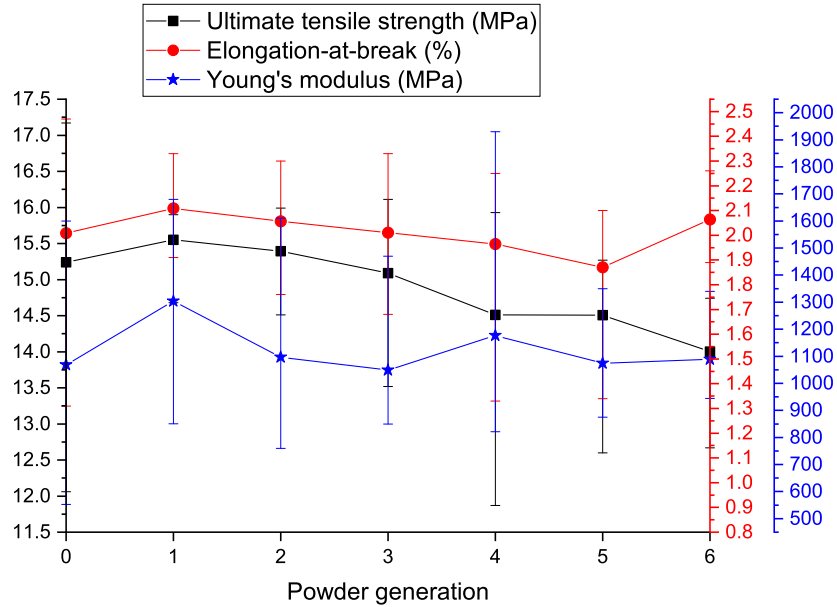


Figure 17: Mean UTS, EaB and YM as functions of powder age. There is no obvious trend for any of the measured mechanical properties. The error bars are the range of measured values, and the lines between data points are included to help guide the reader's eye.

4.7 Statistical analysis of dimensional accuracy and mechanical properties as functions of powder age

Because data for both part accuracy and mechanical properties contained significant uncertainties which make it difficult to determine trends by inspection, further statistical analysis was carried out on these data sets. More specifically, one-way analysis-of-variance (ANOVA) tests were carried out, which were followed by post-hoc Scheffe tests. The ANOVA test determines whether there are statistically significant differences between any of the means within a group of data sets, but is unable to identify which (if any) sets are different. The subsequent Scheffe test performs a pairwise comparison between each data set to identify which specific pairs differ from one another. The results of these statistical tests are summarised in Figure 18.

With the exception of UTS, the ANOVA confirms that there were no significant differences between the tensile properties of the parts made using different powder generations. In the case of UTS, ANOVA identified significant differences in the means of each powder

One way ANOVA set tested	Is it significant at 0.05 level?	Post Hoc test - Scheffe tests
Dimensional accuracy		
Powder Age Shrink	Yes	1U V 2U V 2U 1U 3U V 3U 1U 3U 2U 4U V 4U 1U 4U 2U 4U 3U 5U V 5U 1U 5U 2U 5U 3U 5U 4U 6U V 6U 1U 6U 2U 6U 3U 6U 4U 6U 5U
Powder Age Wall	Yes	1U V 2U V 2U 1U 3U V 3U 1U 3U 2U 4U V 4U 1U 4U 2U 4U 3U 5U V 5U 1U 5U 2U 5U 3U 5U 4U 6U V 6U 1U 6U 2U 6U 3U 6U 4U 6U 5U
Mechanical properties		
Powder Age UTS	Yes	1U V 2U V 2U 1U 3U V 3U 1U 3U 2U 4U V 4U 1U 4U 2U 4U 3U 5U V 5U 1U 5U 2U 5U 3U 5U 4U 6U V 6U 1U 6U 2U 6U 3U 6U 4U 6U 5U
Powder Age EaB	No	1U V 2U V 2U 1U 3U V 3U 1U 3U 2U 4U V 4U 1U 4U 2U 4U 3U 5U V 5U 1U 5U 2U 5U 3U 5U 4U 6U V 6U 1U 6U 2U 6U 3U 6U 4U 6U 5U
Powder Age YM	No	1U V 2U V 2U 1U 3U V 3U 1U 3U 2U 4U V 4U 1U 4U 2U 4U 3U 5U V 5U 1U 5U 2U 5U 3U 5U 4U 6U V 6U 1U 6U 2U 6U 3U 6U 4U 6U 5U
Legend		Significant Not Significant

Figure 18: One-way ANOVA of the effect of powder age on part tensile properties and dimensional accuracy. Each dependent variable is assigned a green "Yes" cell if the ANOVA found there to be a significant difference between the means of each powder age, or a red "No" cell if no significant difference was found. This is followed by a Scheffe test to determine which data sets were significantly different from one another. Each comparison cell for the Scheffe test is highlighted green if the difference between the data sets was significant, and red if it was not. The codes in the Scheffe test table signify the two levels of parameters being examined, e.g. "1U V" is the comparison between once-used powder and virgin powder.

age, but subsequent Scheffe tests could not identify which pairs of data sets were different from one another. The reasons for this are unclear, but it could arise from a lack of statistical power, for example due to the limited number of samples available for comparison (e.g. Used 6 contains only five values of UTS). Without more experimental data, or more sophisticated statistical analyses, it would be unwise to conclude that powder age has no effect on UTS. In contrast, the differences in dimensional accuracy apparent from initial inspection were indeed found to be statistically significant. Interestingly, the shrinkages for powders from generation 3 onwards were all not significantly different from one another, but were almost always significantly different to those from generations 0, 1 and 2. This suggests that increasing crystallinity is indeed the cause of the decrease in shrinkage, as the enthalpy of melting (directly related to crystallinity) was found to plateau from generation 3 onwards. For wall growth, this observation is only true from generation 4, suggesting that if wall growth is also related to crystallinity, it is probably not the only significant factor. On the basis of this statistical analysis, it can be concluded that CP22 PP powder can be recycled up to at least six times through the HSS process without a reduction in the YM and EaB of the parts obtained, but with an increase in their dimensional accuracy.

5 Conclusions and Future Work

In summary, it has been shown that CP22 PP powder can be used in HSS to make good quality parts, albeit with a low build success rate. This was due to a combination of a narrow processing window and difficulties maintaining consistent powder bed temperatures. Nonetheless, it was found that CP22 could subsequently be recycled up to six times through the HSS process with no little-to-no detriment to tensile properties, and no apparent change in polymer chemistry (inferred from molecular weight data). In fact, recycling was actually seen to lead to both an improvement in build success rate, and an increase in the dimensional accuracy of the parts obtained. However, recycling also led to a continuous increase in powder size, and subsequently changes to bulk powder properties (e.g.

density). The practical significance of these changes may depend on the final application for which parts are being built, but in general it is reasonable to conclude that PP is indeed a promising material for use in high-volume manufacturing via HSS, for example to make FMCGs.

However, substantial research work remains to maximise the potential of PP as a material in HSS. Importantly, the high build failure rates seen when using virgin or young CP22 need to be minimised. It is likely that this will be achieved by finding a different PP powder with a wider processing window. Additionally, in order to be truly reflective of high-volume manufacturing, the recycling process needs to be extended past the maximum of seven generations used here. This would also allow it to be established whether some of the ageing-related changes observed here to be continuous (e.g. in particle size) really are continuous at longer ageing times. Finally, an application-focused approach will need to be applied to the changes in part properties observed with increasing age; for example, the probable increase in part porosity associated with decreasing density might increase the rate and extent of solvent uptake, thereby making PP unsuitable for manufacturing liquid containers via HSS. However, while there are clearly several outstanding issues, research into understanding and improving the use of PP powders in HSS should nonetheless be continued in order to help realise the ongoing goal of making AM viable in high-volume manufacturing.

References

- Chen, P., Tang, M., Zhu, W., Yang, L., Wen, S., Yan, C., Ji, Z., Nan, H. and Shi, Y. (2018), “Systematical mechanism of Polyamide-12 aging and its micro-structural evolution during laser sintering,” *Polymer Testing*, Vol. 67 No. March, pp. 370–379.
- Craft, G., Nussbaum, J., Crane, N. and Harmon, J.P. (2018), “Impact of extended sintering times on mechanical properties in PA-12 parts produced by powderbed fusion processes,” *Additive Manufacturing*, Vol. 22 No. June, pp. 800–806.
- Dadbakhsh, S., Verbelen, L., Verkinderen, O., Strobbe, D., Puyvelde, P.V. and Kruth, J.p. (2017), “Effect of PA12 powder reuse on coalescence behaviour and microstructure of SLS parts,” *European Polymer Journal*, Vol. 92 No. December 2016, pp. 250–262.
- Drummer, D., Rietzel, D. and Kühnlein, F. (2010), “Development of a characterization approach for the sintering behavior of new thermoplastics for selective laser sintering,” *Physics Procedia*, Vol. 5 No. PART 2, pp. 533–542.
- Ellis, A., Brown, R. and Hopkinson, N. (2015a), “The effect of build orientation and surface modification on mechanical properties of high speed sintered parts,” *Surface Topography: Metrology and Properties*, Vol. 3 No. 3.
- Ellis, A., Hartley, L. and Hopkinson, N. (2015b), “Effect of Print Density on the Properties of High Speed Sintered Elastomers,” *Metallurgical and Materials Transactions A: Physical Metallurgy and Materials Science*, Vol. 46 No. 9, pp. 3883–3886.
- Ellis, A., Noble, C.J., Hartley, L., Lestrangle, C., Hopkinson, N. and Majewski, C. (2014a), “Materials for high speed sintering,” *Journal of Materials Research*, Vol. 29 No. 17, pp. 2080–2085.
- Ellis, A., Noble, C.J. and Hopkinson, N. (2014b), “High Speed Sintering: Assessing the influence of print density on microstructure and mechanical properties of nylon parts,” *Additive Manufacturing*, Vol. 1, pp. 48–51.

- Fox, L., Ellis, A. and Hopkinson, N. (2015), "Use of an Alternative Ink in the High Speed Sintering Process," *Solid Freeform Fabrication Proceedings*, pp. 456–463.
- Fu, X., Huck, D., Makein, L., Armstrong, B., Willen, U. and Freeman, T. (2012), "Effect of particle shape and size on flow properties of lactose powders," *Particuology*, Vol. 10 No. 2, pp. 203–208.
- Funk, C.V., Koreltz, M.S. and Billovits, G.F. (2016), "Diluent selection for Nylon 11 and Nylon 12 thermally induced phase separation systems," *Journal of Applied Polymer Science*, Vol. 43237, pp. 1–10.
- Hopkinson, N. and Dickens, P. (2003), "Analysis of rapid manufacturing - Using layer manufacturing processes for production," *Proceedings of the Institution of Mechanical Engineers, Part C: Journal of Mechanical Engineering Science*, Vol. 217 No. 1, pp. 31–40.
- Hopkinson, N. and Erasenthiran, P. (2004), "High Speed Sintering – Early Research into a New Rapid Manufacturing Process," *Solid Freeform Fabrication Symposium Proceedings*, pp. 312–320.
- Ituarte, I.F., Wiikinkoski, O. and Jansson, A. (2018), "Additive manufacturing of polypropylene: A screening design of experiment using laser-based powder bed fusion," *Polymers*, Vol. 10 No. 12.
- Kleijnen, R.G., Schmid, M. and Wegener, K. (2016), "Nucleation and impact modification of polypropylene laser sintered parts," *AIP Conference Proceedings*, Vol. 1779 No. October 2016.
- Ligon, S.C., Liska, R., Stampfl, J., Gurr, M. and Mülhaupt, R. (2017), "Polymers for 3D Printing and Customized Additive Manufacturing," *Chemical Reviews*, Vol. 117 No. 15, pp. 10212–10290.
- Majewski, C.E., Oduye, D., Thomas, H.R. and Hopkinson, N. (2008), "Effect of infra-red power level on the sintering behaviour in the high speed sintering process," *Rapid Prototyping Journal*, Vol. 14 No. 3, pp. 155–160.

- O'Connor, H.J., Dickson, A.N. and Dowling, D.P. (2018), "Evaluation of the mechanical performance of polymer parts fabricated using a production scale multi jet fusion printing process," *Additive Manufacturing*, Vol. 22 No. May, pp. 381–387.
- Pham, D.T., Dotchev, K.D. and Yusoff, W.A.Y. (2008), "Deterioration of polyamide powder properties in the laser sintering process," *Proceedings of the Institution of Mechanical Engineers, Part C: Journal of Mechanical Engineering Science*, Vol. 222, pp. 2163–2176.
- Thomas, H.R., Hopkinson, N. and Erasenthiran, P. (2006), "High speed sintering - Continuing research into a new rapid manufacturing process," *17th Solid Freeform Fabrication Symposium, SFF 2006*, pp. 682–691.
- Wegner, A. (2016), "New polymer materials for the laser sintering process: Polypropylene and others," *Physics Procedia*, Vol. 83, pp. 1003–1012.
- Wegner, A. and Ünlü, T. (2016), "Powder Life Cycle Analyses for a New Polypropylene Laser Sintering Material," *Proceedings of the 27th Annual International Solid Freeform Fabrication Symposium: Additive Manufacturing Conference*, Vol. 27, pp. 834–846.
- Wudy, K. and Drummer, D. (2019), "Aging effects of polyamide 12 in selective laser sintering : Molecular weight distribution and thermal properties," *Additive Manufacturing*, Vol. 25 No. November 2018, pp. 1–9.
- Zhu, W., Yan, C., Shi, Y., Wen, S., Liu, J. and Shi, Y. (2015), "Investigation into mechanical and microstructural properties of polypropylene manufactured by selective laser sintering in comparison with injection molding counterparts," *Materials and Design*, Vol. 82, pp. 37–45.